Resonant waveguide–grating switching device with nonlinear optical material

Robert R. Boye, Richard W. Ziolkowski, and Raymond K. Kostuk

The design and analysis of a dielectric guided-mode resonance filter (GMRF) utilizing a nonlinear material for the waveguide is presented. Small changes to the parameters of a GMRF have a large impact on its resonance. A nonlinear material can provide a small change in the refractive index of the waveguide, altering the resonance of the device and resulting in modulation of the transmitted and reflected output of the filter. Numerical results show that nonlinear switching from 100% transmission to 100% reflection can be accomplished with less than 100 kW/cm^2 using a simple design. © 1999 Optical Society of America

OCIS codes: 230.0230, 050.1950, 130.3120, 190.4360, 230.3990, 260.5740.

1. Introduction

In this paper we present the design of a guided-mode resonance filter (GMRF) combined with a nonlinear optical waveguide to form a device that can modulate the transmitted and reflected fields. Therefore the filter can function as a switch that changes state with the input by using the narrow resonance characteristic of the GMRF and the small change to the refractive index that results when the nonlinear material is illuminated. Nonlinear effects typically require high incident intensities to produce significant changes in material optical properties. By using a device that is sensitive to small changes in these properties, a lower input intensity can produce a large change in the device output. Rigorous coupled-wave analysis (RCWA)[1,2] is used to analyze the resonance of the GMRF as well as the effects of the refractive-index changes. Finite-difference time-domain (FDTD) modeling[3,4] is used to complement the RCWA by determining field strengths within the GMRF. In addition, FDTD provides information on the temporal evolution of the fields within the device to determine the limits of the filter switching speed. We present an example design that switches from 100% transmission to 100% reflection over a relatively small range of input optical intensities.

Anomalous output spectra from gratings were first observed by Wood.[5] Although some of Wood's observations were found to be Rayleigh wavelength anomalies, Hessel and Oliner[6] provided the first description of resonance anomalies explaining the remaining phenomena. Mashev and Popov[7] reported the experimental observation of resonance anomalies using an ion-milled grating in conjunction with an ion-exchanged waveguide. The analysis of all dielectric GMRF's[8,9] has led to a large number of design variations and possibilities,[10,11] and recent results have shown high-efficiency devices utilizing a simple design.[12] Possible applications have also expanded from simple wavelength filtering to include laser mirrors,[13] document security,[14] and modulators.[15]

2. Theory and Device Design

A GMRF consists of a grating and waveguide structure that allows light diffracted by the grating to couple to a mode of the waveguide. Figure 1 shows an example using a binary grating on the surface of a waveguide. The coupling between the diffracted energy and waveguide mode leads to a resonant behavior resulting in rapid variations in the amplitudes of the propagating waves, known as resonance anomalies.[9] The eigenvalue equation for the TE field within the waveguide is used in conjunction with the

The authors are with the Optical Sciences Center, University of Arizona, Tucson, Arizona 85721-0001. R. W. Ziolkowski and R. K. Kostuk are with the Department of Electrical and Computer Engineering. The e-mail address for R. R. Boye is rrboye@ece.arizona.edu.

Received 4 February 1999; revised manuscript received 6 April 1999.

0003-6935/99/245181-05$15.00/0

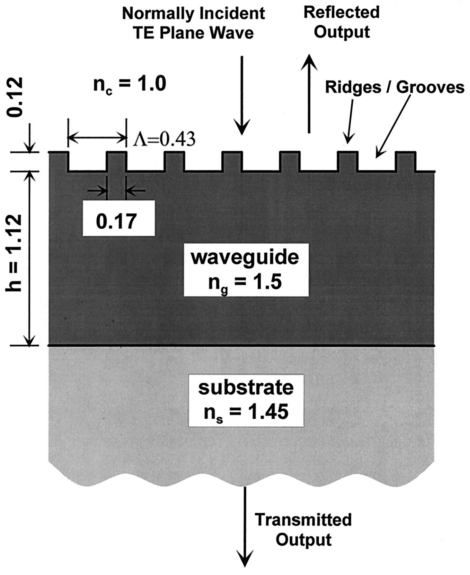

Fig. 1. Design used for analysis. The input is assumed to be a normally incident TE wave, and all dimensions are given in micrometers.

relation for the modified propagation constant to locate the resonances[8]:

$$\tan(\kappa_i h) = \frac{\kappa_i(\gamma_i + \delta_i)}{\kappa_i^2 - \gamma_i\delta_i}, \tag{1}$$

where $\kappa_i = (n_g^2k^2 - \beta_i^2)^{1/2}$, $\gamma_i = (\beta_i^2 - n_c^2k^2)^{1/2}$, and $\delta_i = (\beta_i^2 - n_s^2k^2)^{1/2}$ are the transverse components of the propagation vectors for the waveguide layer of width h, the cover, and the substrate, respectively, with $k = 2\pi/\lambda$. The propagation constant of the waveguide is related to the grating parameters by

$$\beta_i = k(n_g \sin\theta - i\lambda/\Lambda), \tag{2}$$

where θ is the incident angle in the cover and Λ is the period of the grating. Equation (2) shows how several parameters including wavelength, incident angle, grating period, and refractive index affect the resonance of a GMRF. Here we are taking advantage of the direct relation between the waveguide index n_g and the propagation constant to affect the filter resonance and modulate the output fields. To use the GMRF to modulate the incident light beam, an intensity-dependent refractive index is substituted for n_g:

$$n_g = n_0 + n_2I, \tag{3}$$

where the nonlinear index n_2 (in square meters per kilowatt) is related directly to the third-order susceptibility $\chi^{(3)}$ esu by the relation

$$n_2 = 4\pi^2\,\mathrm{Re}(\chi^{(3)})/n_0^2. \tag{4}$$

In addition, a subwavelength period grating is used to ensure that only the zero-order waves propagate outside the device maximizing its efficiency.

The GMRF combines the nonlinear refractive index and subwavelength period grating as shown in Fig. 1 and includes several important features. First, the refractive index of the waveguide and the substrate are chosen to keep the resonance peak narrow while the incident, or cover, material is assumed to be air. The substrate is assumed to be fused silica ($n_s = 1.45$) to provide a low-loss material with high surface quality to avoid scattering. The waveguide is then chosen to have a higher index of $n_g = 1.5$ and a width of $h = 1.12$ μm, resulting in single-mode operation with the desired narrow resonance.

One aspect of the GMRF design that is not included in this analysis is the material loss. Both absorption and scattering adversely affect the resonance of GMRF's, but the design here has material with low loss to minimize these effects. Second, the subwavelength period grating is designed with a duty cycle and depth that would approximate a single-layer quarter-wave antireflection (AR) coating. The AR design serves two purposes. By reducing off-resonance reflections, the contrast of the intensity modulation is maximized. Also, the intensity within the device is increased and produces a larger refractive-index change as shown in Eq. (3). With an incident TE field, the effective index of the grating is defined as[16]:

$$n_{\mathrm{eff}} = (f_1\epsilon_1 + f_2\epsilon_2)^{1/2}, \tag{5}$$

where f_i and ϵ_i are the duty cycle and dielectric constant, respectively, of the two materials comprising the grating. The required refractive index for a single-layer AR coating is the square root of the product of the refractive index of the incident medium and the waveguide. Use of Eq. (5) and the required effective index for an AR effect, the duty cycle of the grating can be found. The depth of the grating is then set equal to a quarter-wave of the resonance wavelength to provide the AR coating. The actual grating ridge width is set to 0.17 μm and the grating depth to 0.12 μm to accommodate a grid consisting of square cells whose side length is 10 nm within the FDTD model. This provides an excellent representation of the GMRF without the need for excessive computation time. Finally, a material for the waveguide that has the desired linear index [$n_0 = 1.5$ in Eq. (3)] and a large nonlinear characteristic is required to produce the modulation effect. For this design, a semiconductor-doped glass (SDG) is assumed. SDG's have the potential for exhibiting enhanced third-order susceptibilities because of the three-dimensional confinement of semiconductor microcrystallites within a glass host material.[17,18] A reported value of $\chi^{(3)} = 4 \times 10^{-7}$ esu (Ref. 17) is used to determine the nonlinear index n_2. The resonance of the GMRF, assuming constant refractive indices, is shown in Fig. 2 as a function of the illumination wavelength. The result shown in Fig. 2 is found using the RCWA. Despite the lack of propagating orders outside of the device, the RCWA model retains 11 total orders to ensure that the effects of evanescent orders are included.

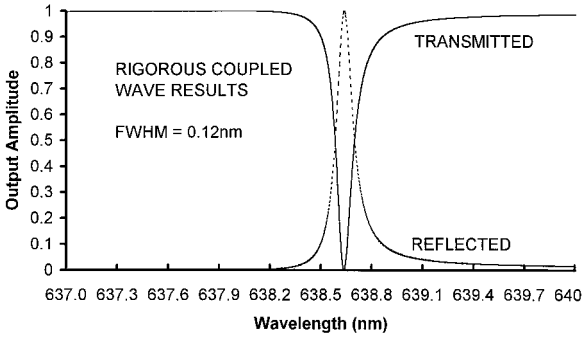

Fig. 2. RCWA shows the resonance of the device assuming a constant index. The resonance wavelength does not exactly match the wavelength of minimum reflection resulting from the approximate AR coating provided by the grating.

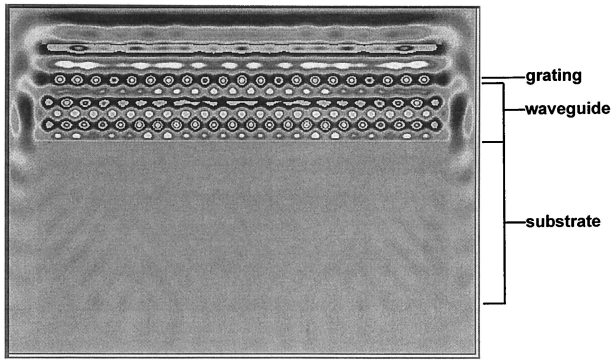

Fig. 4. Gray-scale image of the field amplitude distribution calculated by FDTD modeling. Large positive amplitudes are white and large negative amplitudes are black.

3. Device Analysis and Performance

The first step in the analysis is to determine the refractive-index change that is required to change the resonance properties of the device and modulate the transmitted and reflected outputs while holding the wavelength constant at 638.4 nm. The RCWA results [Fig. 3(a)] show that an extremely large refractive-index change in the ridges of the grating is required, >0.1, to change the device outputs. The refractive index of the ridges of the grating affects the diffraction efficiency of the grating, but the period of the grating determines the direction (or phase) of the diffracted waves and their coupling to the waveguide mode. Within the waveguide, refractive-index variations have a much larger impact on the resonance of the GMRF. Figure 3(b) shows how small changes of the waveguide index, $\sim 10^{-4}$, impact the resonance; therefore the nonlinear material is used only within the waveguide. The propagation vector of the waveguide mode is related directly to the index of the waveguide and affects the resonance behavior of the GMRF. It should be noted that small deviations from the desired linear refractive index n_0 will change the resonance as well. Controlling the refractive index of a SDG to $<10^{-4}$ is impractical, so wavelength or angle tuning would be necessary in practice.

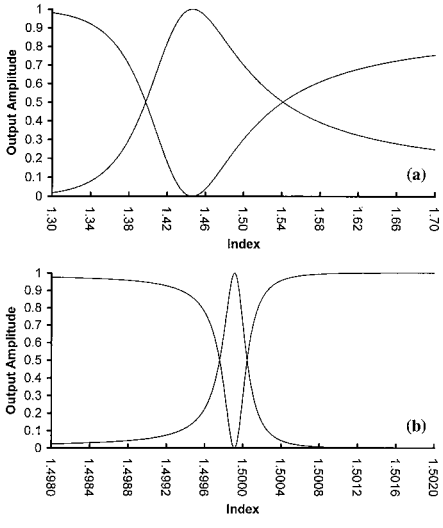

Fig. 3. Effect of index changes on the resonance. (a) Changing the index of the grating ridges requires a large index change to create noticeable changes in the device output. (b) Conversely, the waveguide index has a large influence over the output. The wavelength was held constant just off resonance at 638.4 nm.

To determine the incident intensity needed for the index changes shown in Fig. 3(b), the field strength inside the waveguide must be determined. FDTD modeling is used to calculate the field amplitude within the device as a function of the incident amplitude. The results from the analysis of the GMRF using FDTD with an incident-field amplitude of unity are shown in Fig. 4 where the gray scale corresponds to a field amplitude ranging from 2.5 to -2.5 times the incident field. A complex interference pattern is formed within the waveguide. The forward- and backward-propagating waves interfere with one another as well as with the fields diffracted by the grating. The resultant field distribution within the waveguide produces corresponding variations in the nonlinear refractive index that are then related directly to the incident field. Representing the refractive-index changes in the RCWA model requires splitting the waveguide into many layers (ten layers are used here) and using sampled field values derived from the FDTD analysis and Eq. (3) to determine the refractive-index profile in each layer. Several FDTD simulations were performed to ensure that the calculated field values sampled from the center of the GMRF closely approximate the results from an infinite grating (i.e., without significant edge effects) while using a minimum number of grating periods to reduce the FDTD computation time.

The FDTD simulator was based on the standard staggered grid, leap-frog in-time Yee algorithm.[3,19] The FDTD simulation space was truncated with Berenger's perfectly matched layer absorbing boundary condition.[3,19] The simulation region consisted of 602×1030 square cells ($\delta = 10$ nm), including 20-cell perfectly matched layer regions. The time step was selected according to the Courant stability condition[3,19]: $\delta t = \delta/c\sqrt{2} = 23.57 \times 10^{-18}$ s. The ap-

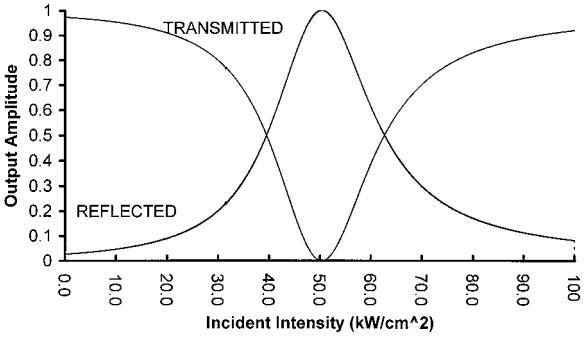

Fig. 5. Output of the GMRF versus input intensity with a normally incident TE plane wave.

propriate dielectric permittivity is specified in each simulation cell. Note that only linear permittivities were considered in the GMRF FDTD simulations to simplify the resulting device analysis. A full nonlinear material FDTD model of the GMRF was beyond the scope of the present study and will be implemented in the future. The initial field is generated from a total field and scattered field interface[3,19] above the grating. The desired electric field values are obtained at specified points throughout the simulation region.

The resulting RCWA model of the GMRF consists of the original grating (no nonlinear material is assumed within the grating) and the ten layers of the waveguide. Each of these ten layers is modeled with a square-wave refractive-index profile with both the high and low refractive indices now dependent on the incident field. The layered waveguide model of the GMRF was evaluated with RCWA with the wavelength held constant (at 638.4 nm) while the incident intensity was varied. Figure 5 shows how the transmission and reflection of the device change with increasing input intensity. The entire resonance peak is spanned by changing the intensity by 100 kW/cm^2, and only 25.3 kW/cm^2 is required to transition from the 10% to 90% reflection levels.

Another important aspect of the nonlinear GMRF performance that can be determined is the factor that limits the modulation rate. There are two main factors that affect the response time of the filter: the time required for the fields to reach equilibrium after a wave is incident on the device and the response of the nonlinear material. FDTD analysis is used to find the temporal response of the fields. Figure 6 shows the field amplitude at a sample point within the waveguide. Large variations in the field amplitude occur as the fields interfere until an equilibrium value is reached after approximately 50 fs. The FDTD simulator was run for 3000 time steps to produce Fig. 6. Longer simulation times showed only minor variations in the resulting field amplitudes at later times. The results shown in Fig. 6 adequately characterize the settling time as 50 fs in the device. In comparison, reported response times for SDG's are in the picosecond and nanosecond range.[18] Therefore the material response limits the switching speed of this nonlinear GMRF design.

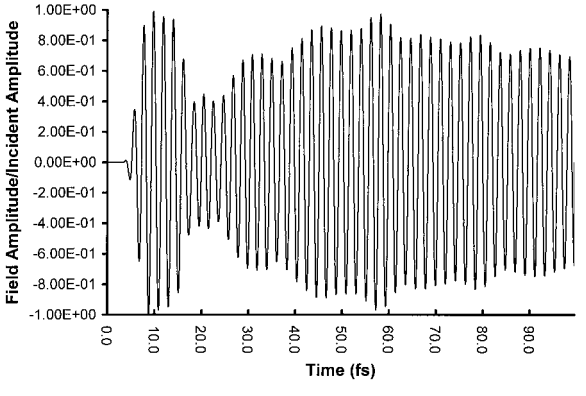

Fig. 6. FDTD predicted time dependence of the field amplitude at a sample point within the waveguide. Large deviations occur as the interference pattern develops, but they settle out in approximately 50 fs.

4. Conclusions

In conclusion, the design of a GMRF utilizing a nonlinear material has been presented. Index changes are required within the waveguide to produce a modulation of the transmitted and reflected outputs. With FDTD analysis, the field profile within the device and subsequent index variations were evaluated. Also the modulation rate of the GMRF was found to be limited by the material response. The RCWA simulator was used to determine the effect of the index variations on the behavior of the GMRF, and it was found that a change in the incident intensity of 100 kW/cm^2 was required to cover the entire resonance peak.

References

1. M. G. Moharam, E. B. Grann, D. A. Pommet, and T. K. Gaylord, "Formulation for stable and efficient implementation of the rigorous coupled-wave analysis of binary gratings," J. Opt. Soc. Am. A **12,** 1068–1076 (1995).
2. M. G. Moharam, E. B. Grann, D. A. Pommet, and T. K. Gaylord, "Stable implementation of the rigorous couple-wave analysis for surface-relief gratings: enhanced transmittance matrix approach," J. Opt. Soc. Am. A **12,** 1077–1086 (1995).
3. A. Taflove, *Computational Electrodynamics* (Artech House, Norwood, Mass., 1995).
4. J. B. Judkins and R. W. Ziolkowski, "Finite-difference time-domain modeling of nonperfectly conducting metallic thin-film gratings," J. Opt. Soc. Am. A **12,** 1974–1983 (1995).
5. R. W. Wood, "On a remarkable case of uneven distribution of light in a diffraction grating spectrum," Philos. Mag. **4,** 396–402 (1902).
6. A. Hessel and A. A. Oliner, "A new theory of Wood's anomalies on optical gratings," Appl. Opt. **4,** 1275–1297 (1965).
7. L. Mashev and E. Popov, "Zero order anomaly of dielectric coated gratings," Opt. Commun. **55,** 377–380 (1985).
8. R. Magnusson and S. S. Wang, "New principle for optical filters," Appl. Phys. Lett. **61,** 1022–1024 (1992).
9. S. S. Wang and R. Magnusson, "Theory and applications of guided-mode resonance filters," Appl. Opt. **32,** 2606–2613 (1993).
10. S. S. Wang and R. Magnusson, "Multilayer waveguide-grating filters," Appl. Opt. **34,** 2414–2420 (1995).

11. S. Peng and G. M. Morris, "Resonant scattering from two-dimensional gratings," J. Opt. Soc. Am. A **13,** 993–1005 (1996).
12. Z. S. Liu, S. Tibuleac, D. Shin, P. P. Young, and R. Magnusson, "High-efficiency guided-mode resonance filter," Opt. Lett. **23,** 1556–1558 (1998).
13. I. A. Avrutskii and V. A. Sychugov, "Reflection of a Gaussian light beam from the surface of a corrugated waveguide," Sov. J. Quantum. Electron. **16,** 1558–1559 (1986).
14. M. T. Gale, K. Knop, and R. Morf, "Zero-order diffractive microstructures for security applications," in *Optical Security and Anticounterfeiting Systems*, W. F. Fagan, ed., Proc. SPIE **1210,** 83–89 (1990).
15. A. Sharon, D. Rosenblatt, A. A. Friesem, H. G. Weber, H. Engel, and R. Steingrueber, "Light modulation with resonant grating-wavelength structures," Opt. Lett. **21,** 1564–1566 (1996).
16. M. Born and E. Wolf, *Principles of Optics* (Pergamon, New York, 1980).
17. S. Ohtsuka, T. Koyama, K. Tsunetomo, H. Nagata, and S. Tanaka, "Nonlinear optical property of CdTe microcrystallites doped glasses fabricated by laser evaporation method," Appl. Phys. Lett. **61,** 2953–2954 (1992).
18. B. Yu, C. Zhu, H. Xia, H. Chen, and F. Gan, "Optical nonlinearities of PbSe microcrystallites doped in glass," J. Mater. Sci. Lett. **16,** 2001–2004 (1997).
19. A. Taflove, *Advances in Computational Electrodynamics* (Artech House, Norwood, Mass., 1998).